JACS
JOURNAL OF THE AMERICAN CHEMICAL SOCIETY
Article
pubs.acs.org/JACS

Role of Tricoordinate Al Sites in CH_3ReO_3/Al_2O_3 Olefin Metathesis Catalysts

Maxence Valla,[†] Raphael Wischert,[†] Aleix Comas-Vives,[†] Matthew P. Conley,[†] René Verel,[†] Christophe Copéret,*[,†] and Philippe Sautet*[,‡]

[†]Department of Chemistry and Applied Biosciences, ETH Zürich, Vladimir Prelog Weg 1-5, 8093 Zurich, Switzerland
[‡]Univ Lyon, Ens de Lyon, CNRS, Université Lyon 1, Laboratoire de Chimie UMR 5182, F 69342 Lyon, France

Supporting Information

ABSTRACT: Re_2O_7 supported on γ-alumina is an alkene metathesis catalyst active at room temperature, compatible with functional groups, but the exact structures of the active sites are unknown. Using CH_3ReO_3/Al_2O_3 as a model for Re_2O_7/Al_2O_3, we show through a combination of reactivity studies, in situ solid-state NMR, and an extensive series of DFT calculations, that μ-methylene structures (Al-CH_2–ReO_3–Al) containing a Re=O bound to a tricoordinated Al (Al_{III}) and CH_2 bound to a four-coordinated Al (Al_{IVb}) are the precursors of the most active sites for olefin metathesis. The resting state of CH_3ReO_3/Al_2O_3 is a distribution of μ-methylene species formed by the activation of the C–H bond of CH_3ReO_3 on different surface Al–O sites. In situ reaction with ethylene results in the formation of Re metallacycle intermediates, which were studied in detail through a combination of solid-state NMR experiments, using labeled ethylene, and DFT calculations. In particular, we were able to distinguish between metallacycles in TBP (trigonal-bipyramidal) and SP (square-pyramidal) geometry, the latter being inactive and detrimental to catalytic activity. The SP sites are more likely to be formed on other Al sites (Al_{IVa}/Al_{IVa}). Experimentally, the activity of CH_3ReO_3/Al_2O_3 depends on the activation temperature of alumina; catalysts activated at or above 500 °C contain more active sites than those activated at 300 °C. We show that the dependence of catalytic activity on the Al_2O_3 activation temperature is related to the quantity of available Al_{III}-defect sites and adsorbed H_2O.

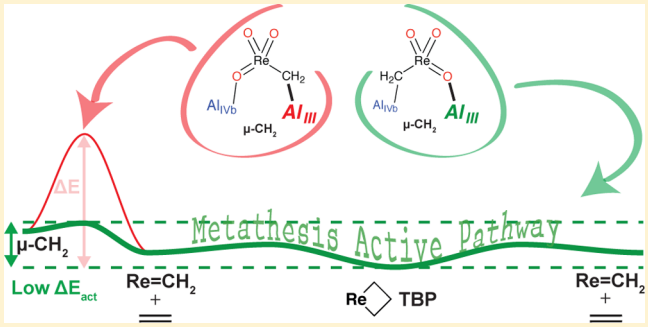

INTRODUCTION

Olefin metathesis is a key reaction for the synthesis of bulk and fine chemicals.[1−4] Subtle tuning of the ligand environment in homogeneous organometallic group 6[5−7] and Ru[8,9] complexes results in high olefin metathesis activities and selectivities. The rational design of these catalysts[10] relies on structure–activity relationships and on the detailed understanding of the key mechanistic steps.[1,2,11−13] The salient features of the Chauvin catalytic cycle are shown in Scheme 1a: olefin coordination to a metal alkylidene, [2 + 2] cycloaddition to form a TBP metallacyclobutane, turnstile isomerization to form the resting state SP metallacyclobutane, cycloreversion from the TBP metallacycle, and olefin decoordination to generate a new metal alkylidene and olefin (Scheme 1a).[14−20] Industrial olefin metathesis catalysts are based on Mo, W, or Re oxides (MO_x) dispersed onto high-surface-area supports.[1,3,4,11−13,21−24] The structures of active sites and reaction intermediates in heterogeneous metathesis catalysts are difficult to determine because only a fraction of the metals sites are catalytically active.[2,3,25,26] Industrial metathesis catalysts are prepared by incipient wetness impregnation of SiO_2 or Al_2O_3 with a MO_x precursor, followed by high-temperature calcination. This step forms isolated metal oxo species in high oxidation states, which under reaction conditions presumably transform into the active alkylidene and metallacyclobutane species.[11−13] The low quantity of active sites prohibits structure–activity optimization of these catalysts and may also explain why most of these catalysts operate above 200 °C. Such a high operating temperature limits functional group compatibility.

The reaction of organometallic alkylidene complexes with partially dehydroxylated oxide supports forms well-defined heterogeneous metathesis catalysts that are active at room temperature and compatible with functionalized olefins.[27−32] This method, referred to as surface organometallic chemistry,[26,33−38] yields catalysts with high concentrations of active sites[27−29,32] that can be characterized by spectroscopic techniques.[19,26,32,39−46] Correlation of the alkylidene active site and catalytic activity allows quantitative assessment of structure–activity relationships,[17,19,20,47] an approach that is similar to homogeneous catalyst optimization.

Re_2O_7/Al_2O_3 is a unique industrial heterogeneous catalyst because it operates at low temperature (25–80 °C),[11,12,28,48,49] and is compatible with functionalized substrates when activated with Me_4Sn.[50,51] The structure of the active site is still a matter of debate, though the Lewis acidic sites in Al_2O_3 appear to play a

Received: January 13, 2016
Published: May 3, 2016

DOI: 10.1021/jacs.6b00447
J. Am. Chem. Soc. 2016, 138, 6774–6785

Scheme 1. General Mechanism, Proposed Active and Inactive Sites, and Resting State[a]

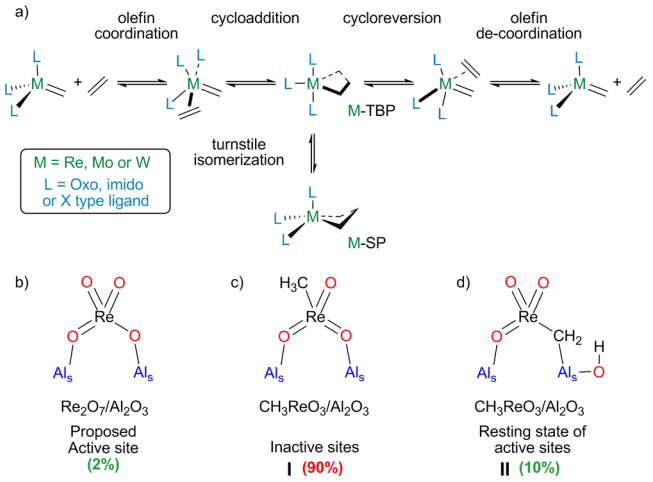

[a](a) General mechanism of olefin metathesis with alkylidene complexes. (b) Proposed active sites of Re_2O_7/Al_2O_3. (c) Inactive sites and (d) resting state of the active sites of CH_3ReO_3/Al_2O_3.

key role in metathesis activity (Scheme 1b).[12,52] Detailed spectroscopic studies on Re_2O_7/Al_2O_3 showed that tetrahedral ReO_4^- coordinated to a pair of Al_{III} and Al_{IV} atoms on the alumina surface are active site precursors. Inactive species are associated with ReO_4^- bound to two Al_{IV} and one Al_{III} atoms in a very distorted geometry where extra oxygen from the surface coordinates to the Re center.[4,47,48]

CH_3ReO_3 supported on alumina and Me_4Sn-activated Re_2O_7/Al_2O_3 have similar reactivity patterns.[28,53−59] The major species (90%) in CH_3ReO_3/Al_2O_3 contains two Re oxo in CH_3ReO_3 coordinated to Al Lewis acid sites (**I**, Scheme 1c) and is inactive in metathesis.[60] The minor species (ca. 10%) in CH_3ReO_3/Al_2O_3 is the μ^2-methylene **II**, which is formed by the activation of a C−H bond in CH_3ReO_3 across an Al−O site (Scheme 1d).[30,31] Labeling and spectroscopic studies showed that **II** is a reservoir of active sites for metathesis.[28] However, neither alkylidenes nor metallacycle metathesis intermediates have been observed in CH_3ReO_3/Al_2O_3. In view of the accepted alkene metathesis mechanism and the characterization of **II**, several questions remain: (i) How does **II** participate in alkene metathesis? (ii) What are the reaction intermediates for this catalyst, and are they observable? (iii) How do the various Al surface sites and their hydration affect the formation and the reactivity of the Re sites?

The present work establishes connections between **II** (the resting state) and the accepted Chauvin metathesis cycle, by combination of experiment and theory. In situ solid-state NMR spectroscopy of CH_3ReO_3/Al_2O_3 in the presence of ^{13}C-dilabeled ethylene shows that TBP and SP metallacycle intermediates are formed. DFT calculations of CH_3ReO_3/Al_2O_3 on model Al_2O_3 surfaces[48,60,61] provide structures and energetics of five possible μ^2-methylene sites as a function of the aluminum site and hydration of the surface. We show that Al_{III} defect sites play a key role in forming metathesis-active Re sites in CH_3ReO_3/Al_2O_3. This study also shows why high-temperature pretreatments of the alumina support are needed to obtain efficient propylene metathesis catalyst: They help generate Al_{III} "defect" sites upon dehydroxylation.

EXPERIMENTAL SECTION

General Methods. All gases were purified by passing over 4 Å molecular sieves and Ru-311 BASF copper catalyst prior to use. Gas chromatography measurements were performed on an Agilent Technologies 7890A GC system equipped with a flame ionization detector and a KCl/Al_2O_3 on fused silica column (50 m x 0.32 mm). Liquid-state NMR spectra were performed on 200, 250, or 300 MHz Bruker spectrometers. Solid-state NMR was performed on a 700 MHz Bruker spectrometer equipped with a 4 mm double-resonance probe head. The ^1H radio frequency (rf) field was set to 100 kHz for cross-polarization (CP-MAS) and heteronuclear correlation (HETCOR) spectroscopy. A 1 s recycle delay was used. HETCOR was recorded with heteronuclear decoupling spinal 64 at the same rf field, and homonuclear ^1H DUMBO decoupling was used. The states-TPPI procedure was applied to achieve quadrature detection in the indirect dimension. Acetonitrile was purchased from Sigma-Aldrich and purified by distillation over CaH_2. Re_2O_7 was purchased from Strem and used as received. Tributylmethyltin and trifluoroacetic anhydride were purchased from Sigma-Aldrich and distilled prior to use. ^{13}C-Labeled ethylene was purchased from Cortecnet and stored over 4 Å molecular sieves and Ru-311 BASF copper catalyst prior to use. Alu C was obtained from Evonik and agglomerated to large particles by suspending in distilled water, drying at 100 °C, and sieving (grain size 250−400 μm) for easier handling. Sieved Al_2O_3 was calcined under a flow of synthetic air for 12 h at 500 °C (ramp of 4 °C·min^{-1}). The atmosphere was removed under vacuum (10^{-5} mBar) while the reactor was still hot, and the alumina was stored in an Ar glovebox.

Synthesis of ^{13}C-Methyltrioxorhenium ($^{13}CH_3ReO_3$) and Methyltrioxorhenium (CH_3ReO_3). These compounds were prepared with 47% yield using a literature procedure.[62]

Activation of Al_2O_3 at Temperatures below 500 °C. Calcined support (500 mg) was rehydrated (with degassed ultra pure water) for 1 h at room temperature and treated under high vacuum at the desired temperature (200−400 °C) for 16 h with a 4 °C min^{-1} ramp.

Preparation of CH_3ReO_3 or $^{13}CH_3ReO_3$ Supported on Al_2O_3: CH_3ReO_3/Al_2O_{3-X} (X = Temperature (°C)). In a 350 mL glass or quartz reactor equipped with a breakable seal, 500 mg of γ-Al_2O_3 was treated under vacuum (10^{-5} mBar) at the desired temperature (200−1000 °C) for 16 h (ramp of 4 °C min^{-1}).[28] CH_3ReO_3 or $^{13}CH_3ReO_3$ (50 mg) was sublimed, and the solid mixture was slowly stirred. After 3 h of reaction at room temperature, the excess molecular complex was removed by reverse sublimation at room temperature under high vacuum (10^{-5} mBar) for 30 min, yielding a dark, colored powder. Elemental analysis for CH_3ReO_3/Al_2O_{3-X}: X = 200 °C, Re = 6.44 wt %; X = 500 °C, Re = 5.63 wt %; X = 700 °C, Re = 6.37 wt %; and X = 900 °C, Re = 6.02 wt %.

Reaction of ^{13}C-Dilabeled Ethylene with CH_3ReO_3/Al_2O_3. CH_3ReO_3/Al_2O_3 (300 mg) was loaded into a reactor of known volume (300 mL). Dilabeled ethylene (0.5 equiv per Re) was added to the powder. The gas phase was analyzed by GC/MS after either 30 min or 15 h to determine the ratio of ethylene isotopomers. CH_3ReO_3/Al_2O_3 reacted with ethylene for 15 h was analyzed by ^{13}C CPMAS solid-state NMR spectroscopy.

In Situ Reaction of ^{13}C-Dilabeled Ethylene with CH_3ReO_3/Al_2O_3 Sealed in a Glass Insert. $CH_3ReO_3/Al_2O_{3\text{-}500}$ (30 mg, 5.1 × 10^{-3} mmol of Re) was loaded into a glass insert fitting into a 4 mm solid-state NMR rotor. ^{13}C-Dilabeled ethylene (2.6 × 10^{-3} mmol of ethylene) was added into the glass insert. The glass insert was flame-sealed and inserted into a 4 mm rotor for solid-state NMR measurements.

Computational Methods. The DFT calculations were performed in the generalized gradient approximation (GGA) using the Perdew−Wang (PW91) functional,[63] as implemented in the VASP 4.6 code.[64,65] The projected augmented wave (PAW) method was adopted.[66] A tight convergence of the plane-wave expansion was obtained with a kinetic energy cutoff of 400 eV, in accordance with the selected PAW atomic radii. The (110) surfaces of γ-Al_2O_3 are based on our previously established models.[65] Test calculations show that 8-layer-thick slabs (unit formula $Al_{32}O_{48}$) yield converged adsorption energies. The Brillouin zone integration was performed with a 3 × 3 × 1 k-point grid

DOI: 10.1021/jacs.6b00447
J. Am. Chem. Soc. 2016, 138, 6774−6785

generated by the Monkhorst−Pack algorithm. Energies were converged when the total energy difference between two steps of the SCF loop was below 1×10^{-6} eV, and residual forces on atoms were converged when below 0.01 eV/Å. To reproduce the properties of extended surfaces, the bottom two layers were kept fixed during the calculations at bulk coordinates, whereas the top layers were allowed to relax. The climbing image nudged elastic band method (CI-NEB) was used to determine the transition states, with sets of 8 images. The so-obtained transition states (TS) guesses were further refined with a quasi-Newton algorithm and validated with a vibrational analysis.[67,68] For NMR calculations, the Materials Studio CASTEP code (version 5.5) was used on the structures optimized with VASP.[69] Carbon and proton chemical shifts were referenced to tetramethylsilane. We used the PBE functional[70,71] and on-the-fly generated pseudopotentials with a cutoff energy of 490 eV. The calculations were carried out on the ETHZ "Brutus" cluster using 8−64 cores. Figures of the structures were produced with the XCrySDen program.[72]

Computational Details of the PDOS Calculations. The contribution of the s and p orbitals of the carbon atom of CH_3ReO_3 to the density of states (DOS) was evaluated on the optimized structures of the molecule, the enolic form, and the μ-methylene and alkylidene species of the grafted structure. The DOS was calculated with VASP using a dense k-point grid ($9 \times 9 \times 1$), and the projected density of states (PDOS) was extracted with the p4vasp program.[72] To assist with the interpretation of the PDOS, molecular orbital calculations were performed for MTO and its enolic tautomer. These calculations were performed with the Gaussian 09 program package[73] using the B3PW91 density functional.[63,74] The LANL2DZ basis set was used[75] for Re, with augmented by f-polarization functions,[76] whereas for C, H, and O, the 6-311++G(d,p) basis set was used instead.

RESULTS

Experimental Studies. *Effect of Al_2O_3 Activation Temperature on the Quantity of Active Sites.* The activity of CH_3ReO_3/Al_2O_3[28] in propene metathesis, and the number of active sites in these catalysts, were determined as a function of the activation temperature of alumina. As the temperature of activation increases the density of surface −OH groups decreases; this behavior is coupled with the generation of highly reactive (defect) Lewis acidic Al-sites.[30,31,77] We prepared CH_3ReO_3/Al_2O_3 on alumina activated at X = 200, 300, 500, 600, 700, 800, and 1000 °C to form $CH_3ReO_3/Al_2O_{3\text{-}X}$. For clarity, in the discussions below, CH_3ReO_3/Al_2O_3 and $^{13}CH_3ReO_3/Al_2O_3$ refer to natural abundance and ^{13}C-enriched CH_3ReO_3, respectively. In all cases, contacting CH_3ReO_3/Al_2O_3 with 450 equiv of propene per Re at 25 °C results in the formation of ethylene and 2-butenes, indicating that all CH_3ReO_3/Al_2O_3 catalysts are active in olefin metathesis. $CH_3ReO_3/Al_2O_{3\text{-}500}$ reaches 10% of propene conversion in less than 50 min. Catalysts prepared on alumina activated above 500 °C display similar catalytic activities (Figure S1). In contrast, catalysts prepared on alumina activated below 500 °C show significantly lower activities. For instance, 80 min is needed for $CH_3ReO_3/Al_2O_{3\text{-}300}$ to reach 10% conversion, whereas 220 min is necessary for $CH_3ReO_3/Al_2O_{3\text{-}200}$ under these conditions.

The quantity of active sites in these catalysts was evaluated by the reaction of ^{13}C-dilabeled ethylene (0.5 equiv per Re) with CH_3ReO_3/Al_2O_3.[56] The amount of ^{13}C incorporated into gas-phase ethylene corresponds to the number of active sites. A plot of the amount of ^{13}C-label detected in the gas phase after 30 min and 16 h of reaction time is given in Figure 1. After 30 min of reaction, more than 8% of the Re sites are active for catalysts prepared on Al_2O_3 activated at or above 500 °C. In contrast, $CH_3ReO_3/Al_2O_{3\text{-}300}$ contains only 3% active sites according to the same titration method. These results parallel the activity of CH_3ReO_3/Al_2O_3 in the metathesis of propene discussed above

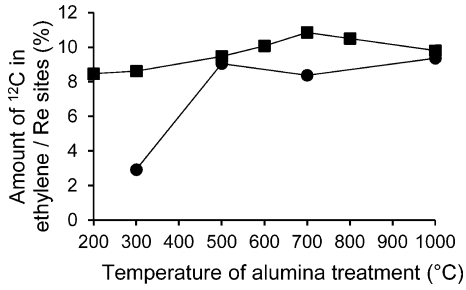

Figure 1. Quantification of ^{12}C in ethylene isotopomers after 30 min reaction time of CH_3ReO_3/Al_2O_3 and ^{13}C-ethylene (●); quantification after 16 h reaction time (■).

and suggest that the performance of the catalyst depends on the level of hydroxylation of the alumina support.[52,78,79] However, titration of active sites carried out after 16 h of reaction shows that all catalysts have roughly the same number of active sites, suggesting a distribution of sites with different activities in CH_3ReO_3/Al_2O_3 depending on the hydroxylation level.

Detection of Reaction Intermediates. The ^{13}C cross-polarization magic angle-spinning (CPMAS) spectrum of $^*CH_3ReO_3/Al_2O_{3\text{-}500}$ contains one signal at 66 ppm with a width at half-maximum ($\nu_{1/2}$) of 2600 Hz and one signal at 30 ppm ($\nu_{1/2}$ = 4000 Hz), assigned to the μ-methylene species **II** and the inactive oxo-species **I**, respectively (Figure S2). The ^{13}C CPMAS spectrum of $^*CH_3ReO_3/Al_2O_{3\text{-}500}$ after contact with natural abundance propene or ethylene (450 equiv per Re) contains the μ-methylene, though with lower intensity (Figure S3), indicating that not all μ-methylene sites participate in the metathesis reaction. The ^{13}C CPMAS spectrum of $CH_3ReO_3/Al_2O_{3\text{-}500}$ after contact with ^{13}C-dilabeled ethylene and removal of the gas phase also contains the μ-methylene signal at 66 ppm, though with a narrower line width ($\nu_{1/2}$ = 1800 Hz) for the μ-methylene species other than $^*CH_3ReO_3/Al_2O_3$ (Figure S4). Interestingly, this μ-methylene species could only be observed at short contact time when using CPMAS techniques. This is probably due to dynamics of the Re sites on the surface. These results support the presence of a distribution of Re sites in CH_3ReO_3/Al_2O_3, some of them being more reactive than others.

NMR signals of Re alkylidenes (expected between 200 and 300 ppm)[80] or metallacycles (two peaks for TBP geometry at ca. 0/100 ppm versus two peaks for SBP at ca. 20−50 ppm) were never observed in any CH_3ReO_3/Al_2O_3 NMR experiment. In the absence of olefins, metallacycle intermediates can decompose to alkylidenes or, in this case, to μ-methylene species **II**. The ^{13}C CPMAS spectrum of $CH_3ReO_3/Al_2O_{3\text{-}500}$ in the presence of ^{13}C-dilabeled ethylene (0.5 equiv per Re) sealed in a glass insert contains signals at 19, 36, 43, 66, and 120 ppm (Figure 2). Signals typical for alkylidenes were not detected (Figure S5). The signal at 66 ppm ($\nu_{1/2}$ = 1900 Hz) corresponds to μ-methylene species **II** having low reactivity toward olefins. The peaks at 120 ppm ($\nu_{1/2}$ = 510 Hz) and 19 ppm ($\nu_{1/2}$ = 520 Hz) are characteristic for the α- and β-carbons of a metallacycle in TBP geometry (Figure 2),[14,15,17,19,81] and those at 43 ($\nu_{1/2}$ = 440 Hz) and 36 ppm ($\nu_{1/2}$ = 1200 Hz) are characteristic for the α- and β-carbons of a metallacycle in SP geometry.[17,19] The blank experiment of Al_2O_3 dehydroxylated at 700 °C contacted with ^{13}C-labeled ethylene exhibits peaks assigned to coordinated, C−H activated, and oligomerized ethylene (Figure S6). These peaks cannot be found in the present NMR (Figure 2) indicating that the observed peaks are due to the reaction of

DOI: 10.1021/jacs.6b00447
J. Am. Chem. Soc. 2016, 138, 6774−6785

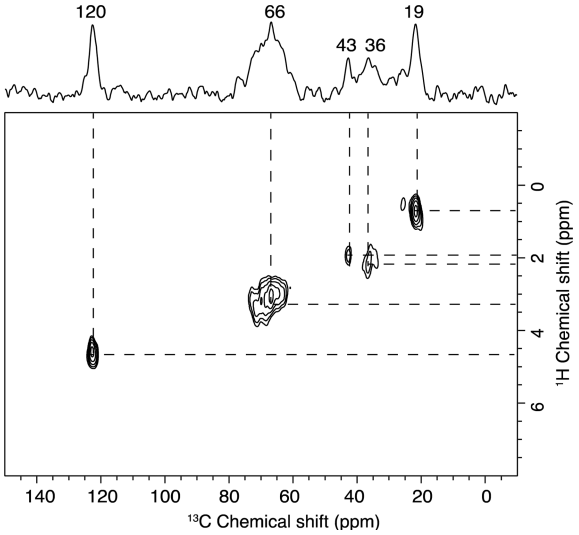

Figure 2. $^{1}H-^{13}C$ HETCOR NMR spectrum of $CH_3ReO_3/Al_2O_{3\text{-}500}$ in the presence of 0.5 equiv of ^{13}C-dilabeled ethylene/Re sealed in a glass insert at 9 kHz spinning speed. DUMBO[82,83] decoupling was applied. The contact time was set to 250 μs, and the recycle delay was set to 1 s.

ethylene with Al surface sites. The assignments of the TBP and SP metallacycles are supported by a 2D $^{1}H-^{13}C$ heteronuclear correlation (HETCOR) spectrum in Figure 2. The cross-peaks between proton and carbon resonances (H/C) at (19/0.4) and (120/4.2) are consistent with their assignment as the α- and β-(carbon/proton) of the TBP metallacyclobutane. In addition, the cross-peaks at (43/1.8) and (36/2.0) support their assignment to the SP metallacycle. The narrow line widths of the peaks corresponding to the TBP and SP metallacycles indicate a narrow site distribution, in contrast to the much broader μ-methylene signal. The absence of alkylidene signals suggests that they are either difficult to observe or less stable than those of the corresponding μ-methylene (or metallacycle).

Computational Studies of CH_3ReO_3 Adsorbed on Activated Al_2O_3. The experimental results discussed above show that μ-methylene species **II** is an active site precursor. **II** is present as a distribution of sites, as shown by titrations and solid-state NMR studies. We investigated the structures, spectroscopic signatures, and reactivity of μ-methylene sites in CH_3ReO_3/Al_2O_3 using computational modeling and compared their stability to that of the corresponding Re oxo bound structures (**I**).

A typical γ-alumina particle contains 110 (74%), 100 (16%), and 111 (10%) facets.[84−86] The model of the fully dehydroxylated 110 facet (**s0**) contains one type of tricoordinate aluminum (Al_{III}) and two types of four-coordinate aluminum sites (Al_{IVa} and Al_{IVb}) per unit cell (Figure 3a). Al_{III} is defined as a defect site because of its low surface density on hydroxylated surfaces; this site is generally occupied by hydroxyl.[59,60] The stability of a surface Re site can be defined by its adsorption energy (E_{ads}) on **s0** as follows:

$$E_{ads} = E(\mathbf{s0} + CH_3ReO_3) - E(CH_3ReO_3) - E(\mathbf{s0}) \quad (1)$$

where $E(\mathbf{s0} + CH_3ReO_3)$, $E(CH_3ReO_3)$, and $E(\mathbf{s0})$ correspond to the electronic energies of CH_3ReO_3 adsorbed on the surface, CH_3ReO_3, and the dehydroxylated alumina surface (**s0**).

Stability of Re Oxo Species on the Fully Dehydrated Alumina Surface. The adsorption of CH_3ReO_3 on Al_{III} and Al_{IVa} centers through one oxo ligand (**0-III** and **0-IVa**) is exoenergetic by −144 and −56 kJ mol^{-1}, respectively (Figure S7a). A similar structure was not obtained on Al_{IVb} because it directly evolved into a structure where two Re═O groups are coordinated to the surface (vide infra, **0-IVa,IVb**). Bis-grafted Re oxo species are referred to as **0-A,B** to indicate to which Al centers (A and B) the oxo groups of CH_3ReO_3 are bound (Figure 3b,c). The most stable species associated with an adsorption energy of −224 kJ mol^{-1} is **0-III,IVb**, which also contains one oxygen atom from the alumina surface coordinated to Re. **0-IVa,IVb** has an adsorption energy of −202 kJ mol^{-1} and also contains an additional surface oxygen atom coordinated to Re, whereas the adsorption energy of **0-IVa,IVa** is only −72 kJ mol^{-1}.

Stability of the μ-Methylene Species on the Fully Dehydrated Alumina Surface. CH_3ReO_3 adsorbs on two Al sites of the fully dehydrated (**s0**) 110 facet to form μ-methylene surface species and a proton on an adjacent O atom (Figure 3b,d).[60] Five μ-methylene adsorbates can form, which differ in the surface aluminum atoms bound to the μ-CH_2 and the oxo ligands. The models for the μ-methylene surface species are referred to as **1-A,B** to indicate that the μ-CH_2 ligand sits on A and the oxo on B (Figure 3b). The structures and adsorption energies of these species are summarized in Table 1 and Figure 3. CH_3ReO_3 preferentially adsorbs on Al_{III} and Al_{IVb} sites with high E_{ads} of −233 and −211 kJ mol^{-1} for **1-III,IVb** and **1-IVb,III**, respectively. CH_3ReO_3 forms less stable surface complexes on sites not involving Al_{III}: E_{ads} for **1-IVa,IVb**, **1-IVb,IVa**, **1-IVa,IVa** are −96, − 129, and −90 kJ mol^{-1}, respectively. In **1-III,IVb**, **1-IVb,III**, and **1-IVa,IVa**, the Re center adopts a pseudotetrahedral geometry with Re−C bond length of 2.00−2.01 Å. In these three structures, two oxo ligands are pointing away from the surface with Re−O bond lengths of ca. 1.71 Å, and one oxo ligand is coordinated to an adjacent aluminum and is elongated to ca. 1.78 Å. The Re centers in **1-IVa,IVb** and **1-IVb,IVa** are pseudo-octahedral because of the presence of two additional dative interactions from surface oxygen atoms.

To summarize, the stability (E_{ads}) of the oxo and μ-methylene species decreases as follows: **1-III,IVb** (−233) > **0-III,IVb** (−224) > **1-IVb,III** (−211) > **0-IVa,IVb** (−202) ≫ **0-III** (−144) > **1-IVb,IVa** (−129) > **1-IVa,IVb** (−96) > **1-IVa,IVa** (−90) > **0-IVa,IVa** (−72) > **0-IVa** (−56). Although the μ-methylene species **1-III,IVb** is the overall most stable structure, a mixture of oxo and methylene species should be present because of the small energy differences between them and the presence of adsorbed water on various Al sites of the initial support. Not surprisingly, monobound species (such as **0-III**) are much less stable than structures in which CH_3ReO_3 interacts with the surface through two or more bonds.

Formation of μ-Methylene Species on the Fully Dehydrated Alumina Surface. Below we refer to $[TS]^{‡}$ as the energy of the transition state structure and $E^{‡}$ as the energy barrier with respect to the preceding intermediate. These energies are defined as follows:

$$[TS]^{‡} = E(\mathbf{\textit{si}} + CH_3ReO_3 + C_2H_4)^{‡} - E(CH_3ReO_3) - E(\mathrm{si}) - E(C_2H_4) \quad (2)$$

$$E^{‡} = [TS]^{‡} - E_{intermediate}(\mathbf{\textit{si}} + CH_3ReO_3 + C_2H_4) \quad (3)$$

where ***si*** is the surface containing ***i*** dissociated water molecules per unit cell. For the interconversion between μ-methylene and

DOI: 10.1021/jacs.6b00447
J. Am. Chem. Soc. 2016, 138, 6774−6785

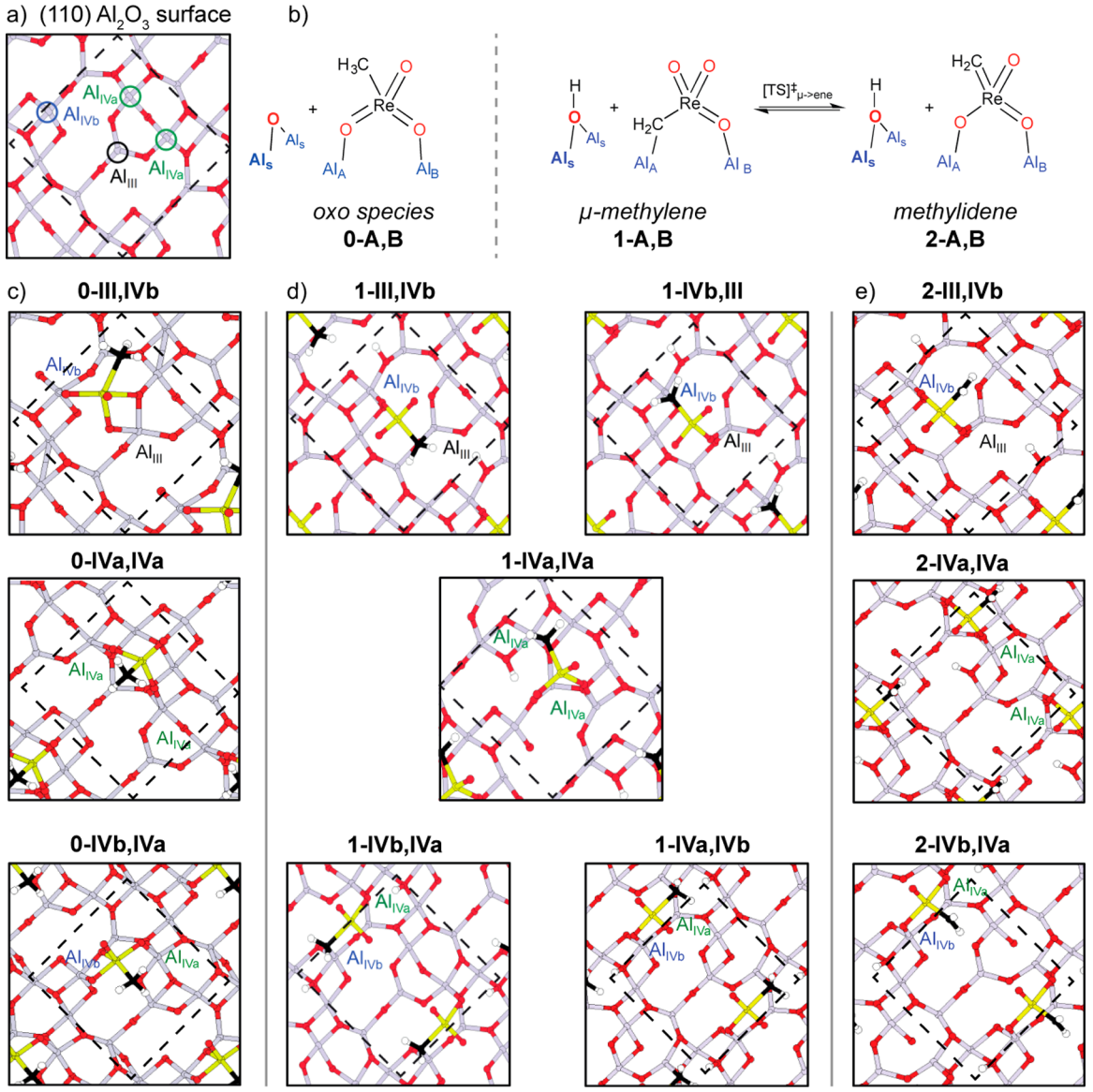

Figure 3. (a) Fully dehydroxylated γ-Al_2O_3 (110) surface. (b) The oxo species (**0-A,B**), the μ-methylene species (**1-A,B**) and its interconversion into the corresponding alkylidene (**2-A,B**). (c) Optimized structures of the oxo-species (**0-A,B**) on different Al site pairs of the fully dehydrated γ-Al_2O_3 (110) surface (**s0**). (d) Optimized structures of the μ-methylene species (**1-A,B**) where A and B correspond to Al sites bound to CH_2 and oxo, respectively. (e) Optimized structures of the alkylidene species (**2-A,B**) (**s0**). Only the two top layers of the periodical slab of the alumina are shown for clarity. The surface unit cell is indicated by a black dashed line. Color code is as follows: Al (Gray), O (red), Re (yellow), C (black), and H (white).

Table 1. Adsorption Sites, Geometry at Re (G), Adsorption Energies (E_{ads}) for the Oxo Species (0-A,B), the μ-Methylene Species (1-A,B) and the Re Methylidene Species (2-A,B) on the Fully Dehydrated γ-Al_2O_3 (110) Surface (s0)[a]

0-A,B	E_{ads}	**1-A,B**	G[c]	E_{ads} (ΔE)[d]	[TS]‡	E‡	**2-A,B**	G[c]	E_{ads} (ΔE)[e]	[TS]‡$_{\mu\rightarrow ene}$	E‡$_{\mu\rightarrow ene}$
IVa,IVb[b]	−202	III,IVb	T	−233 (−31)	−59	143	III,IVb	T	−269 (−36)	−33	200
III,IVb	−224										
III	−144	IVb,III	T	−211 (−67)	−77	67	III,IVb	T	−269 (−58)	−162	49
IVa[b]	−56	IVa,IVa	T	−90 (−34)	−11	45	IVa,IVa	T	−127 (−37)	+5	95
IVa,IVa	−72										
IVa	−56	IVb,IVa	O	−129 (−73)	*f*	*f*	IVb,IVa	O	−151 (−22)	*g*	*g*
IVa,IVb[b]	−202	IVa,IVb	O	−96 (+106)	*f*	*f*	IVb,IVa	O	−151 (−55)	+17	113

[a]Transition state energies [TS]‡ and activation energies E‡ for their interconversion (**0-A,B** to **1-A,B** and **1-A,B** to **2-A,B**) are also given. All energies are in kJ mol^{-1}. Mono grafted **0** species are available in Figure S8. [b]Oxo species precursor of the corresponding μ-methylene. [c]Symmetry of the surface Re species. T and O indicate pseudotetrahedral or octahedral coordination of Re, respectively. [d]The energy in parentheses (ΔE) corresponds to the difference in stability of the μ-methylene and the oxo species: $\Delta E = E_{ads}(\mu\text{-}CH_2) - E_{ads}(\text{oxo})$. [e]The energy in parentheses (ΔE) corresponds to the difference in stability of the methylidene and the μ-methylene species: $\Delta E = E_{ads}(\text{methylidene}) - E_{ads}(\mu\text{-}CH_2)$. [f]Structures not calculated. [g]No transition state could be located.

DOI: 10.1021/jacs.6b00447
J. Am. Chem. Soc. 2016, 138, 6774−6785

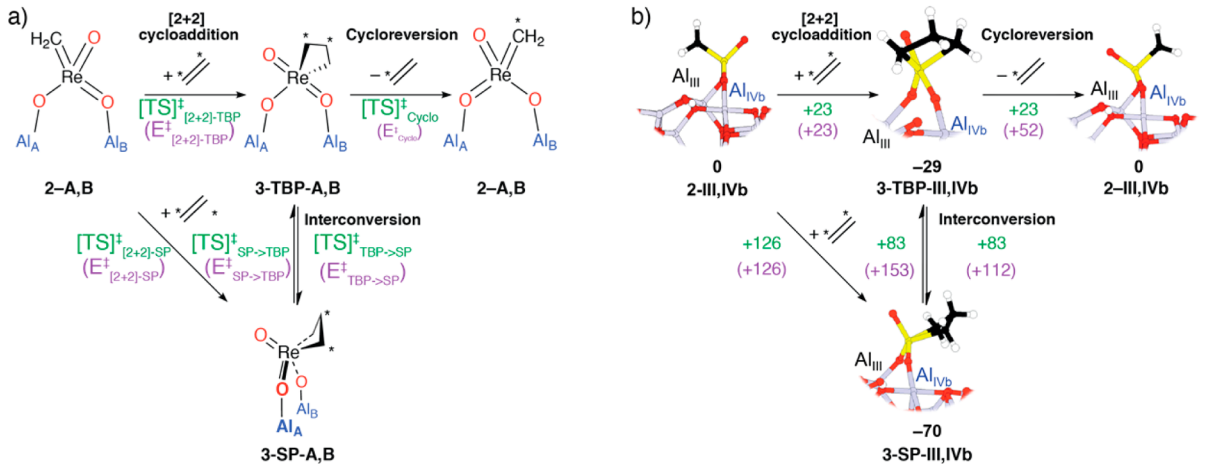

Figure 4. (a) Schematic representation of the metathesis pathway of CH_3ReO_3/Al_2O_3 and ethylene for all sites with the corresponding nomenclature for naming the transition states and corresponding energy barriers. (b) Structures of the metathesis intermediates starting from **2-III,IVb** on **s0**, the most favorable site for metathesis. Transition state energies are in green, and activation energies of the corresponding elementary steps are in purple. The structures of the metathesis intermediate from **2-IVa,IVa** and **2-IVb,IVa** are available in Figures S9 and S10. Transition state structures are available in Figure S11. Energies are in kJ mol^{-1}.

Table 2. Energies of Transition State Structures and Reaction Intermediates with the Corresponding Energy Barriers for Elementary Steps for Ethylene Metathesis on 2 Adsorbed on the Fully Dehydrated γ-Al_2O_3 (110) Surface (s0) (kJ mol^{-1})[a]

A,B	ΔE (2-A,B)[b]	ΔE (3-TBP-A,B)[b]	ΔE (3-SP-A,B)[b]	$[TS]^{\ddagger}_{[2+2]\text{-TBP}}$	$[TS]^{\ddagger}_{[2+2]\text{-SP}}$	$[TS]^{\ddagger}_{TBP\rightarrow SP}$	$E^{\ddagger}_{TBP\rightarrow SP}$	$E^{\ddagger}_{cyclo}$	$E^{\ddagger}_{SP\rightarrow TBP}$
III/IVb	0	−29	−70	+23	+126	+83	+112	+52	+153
IVa/IVa	0	−37	−70	+40	+121	+48	+85	+77	+118
IVb/IVa	0	*b*	−59	*c*	+177	*c*	*c*	*c*	*c*

[a]Energies are referenced according to **2-A,B** for the metathesis pathway and are expressed in kJ mol^{-1}. (E_{ads} are available in Figure S7.) [b]Energy difference between the structure and **2-A,B** in kJ mol^{-1}. [c]The structure or the transition state energies could not be located.

the corresponding methylidene, ethylene was not considered in the transition state calculations.

Table 1 summarizes the reaction energies associated with the formation of μ-methylene species **1** with respect to separated reactants and possible oxo-bound initial states (**0**). Transition states were calculated, starting from oxo-bound species **0** because the coordination of the oxo ligand is likely barrierless (for transition state structures, see Figure S8). For the formation of the most stable surface species **1-III,IVb**, starting from **0-IVa,IVb**, a transition state was located at an energy $[TS]^{\ddagger} = -59$ kJ mol^{-1} below separated reactants (CH_3ReO_3 and Al_2O_3). Although the energy gain from **0-IVa,IVb** is 31 kJ mol^{-1}, the energy barrier is rather high, $E^{\ddagger} = 143$ kJ mol^{-1}. For **1-IVb,III**, a transition state was located starting from **0-III** at $[TS]^{\ddagger} = -77$ kJ mol^{-1} in a process associated with a reaction energy of −67 kJ mol^{-1} and an energy barrier of $E^{\ddagger} = +67$ kJ mol^{-1}. The formation of **1-IVa,IVa** from **0-IVa** is associated with a reaction energy of −34 kJ mol^{-1} and an energy barrier of $E^{\ddagger} = 45$ kJ mol^{-1}. The formation of **1-IVa,IVb** and **1-IVb,IVa** was not investigated because they are much less stable than **0-IVa,IVb**. Overall, **1-IVb,III** and **1-IVa,IVa** are kinetically accessible, whereas other species, including the very stable **1-III,IV**, are much less likely on the **s0** surface. This computational data shows that mixtures of **0** and **1** species will be formed on the alumina surface, consistent with experiment.

Stability and Structures of Methylidene Species on Fully Dehydrated Alumina. Alkylidene (here methylidene) intermediates are expected in metathesis catalysts. The structures of methylidenes **2-A,B** are shown in Figure 3. The interconversion of **1-A,B** to **2-A,B** conserves the geometry at Re: **2-III,IVb** and **2-IVa,IVa** are tetrahedral and **2-IVb,IVb** is octahedral. **2-A,B** has a short Re−C bond distance (1.87−1.88 Å), significantly shorter than in **1-A,B** (see Tables S1 and S2 for more details). In all cases, methylidene are slightly more stable than corresponding μ-methylene species (Table 1). **2−III,IVb** ($E_{ads} = -269$ kJ mol^{-1}) is 36 kJ mol^{-1} more stable than **1-III,IVb** and 58 kJ mol^{-1} more stable than **1-IVb,III**. Similarly, **2-IVa,IVa** ($E_{ads} = -127$ kJ mol^{-1}) is 37 kJ mol^{-1} more stable than **1-IVa,IVa**. Octahedral **2-IVb,IVa** ($E_{ads} = -151$ kJ mol^{-1}) is 22 kJ mol^{-1} more stable than **2-IVb,IVa** and 55 kJ mol^{-1} more stable than **2-IVa,IVb**.

Interconversion between μ-Methylene and Methylidene Species on Dehydrated Alumina. Forming methylidene involves the decoordination of μ-methylene ligand, rotation, and coordination of an additional Re═O unit to the surface. The energy barrier ($E^{\ddagger}_{\mu\rightarrow ene}$) for interconversion depends on the Al sites. The transition state structures are given in Figure S8. The energy barrier for the formation of **2-III,IVb** is 200 kJ mol^{-1} above **1-III,IVb** (Table 1), suggesting that these sites probably do not interconvert at room temperature. In contrast, $E^{\ddagger}_{\mu\rightarrow ene}$ to form **2-III,IVb** from **1-IVb,III** is only 49 kJ mol^{-1}. The weaker Lewis acidity of Al_{IVb} compared to the Al_{III} site probably allows easier decoordination of the μ-methylene, hence the lower barrier to form **2-III,IVb**. **1-IVa,IVa** and **1-IVa,IVb** form **2-IVa,IVa** and **2-IVb,IVa** with energy barriers of 95 and 113 kJ mol^{-1}, respectively. In addition, **2-IVa,IVa** and **2-IVb,IVa** are less stable than **2-III,IVb**, suggesting that these sites may not play an important role in metathesis.

*Reactivity of **2-A,B** with Ethylene.* [2 + 2]-Cycloaddition of **2-A,B** and ethylene forms the TBP or SP metallacyclobutanes **3-TBP-A,B** and **3-SP-A,B** shown in Figure 4a (see Scheme S1 and Figure S7b for details). **3-TBP-A,B** contains two Re═O axial

DOI: 10.1021/jacs.6b00447
J. Am. Chem. Soc. 2016, 138, 6774−6785

Table 3. Adsorption Sites, Geometry at Re (G), and Adsorption Energies (E_{ads}) for the Oxo Species (0-A,B), μ-Methylene Species (1-A,B), and Methylidene Species (2-A,B) on Partially Hydrated γ-Al_2O_3 (110) Surfaces (s1 and s2) and Transition State Energies and Barriers for the Their Interconversion[a]

surface	**0-A,B**	G^c	E_{ads} (ΔE)[d]	**1,A,B**	G^c	E_{ads} (ΔE)[e]	$[TS]^{\ddagger}$	$E^{\ddagger}$
s1	IVa,IVb[b]	P	−91 (-202)	III,IVb	T	−203 (−112)	+25	116
s1	III/IVb	P	−184 (-224)					
s1	III[b]	P	116 (−144)	IVb,III	T	−140 (−24)	−95	21
surface	**1-A,B**	G^c	E_{ads}[f]	**2-A,B**	G^c	E_{ads} (ΔE)[g]	$[TS]^{\ddagger}_{\mu\rightarrow ene}$	$E^{\ddagger}_{\mu\rightarrow ene}$
s1	III,IVb	T	−203 (−233)	III,IVb	T	−193 (+10)	−4	+199
s2	III,IVb	P	−104	III,IVb	P	−136 (−32)	+52	+156
s1	IVb,III	T	−140 (−211)	III,IVb	T	−193 (−53)	−126	+14
s2	IVb,III	P	−97	III,IVb	P	−136 (−39)	−77	+20
s1	IVa,IVa	T	−14 (−90)	IVa,IVa	T	−51 (−37)	+52	+66
s2	[h]	[h]	[h]	IVa,IVa	[h]	[h]	[h]	[h]
s1	IVb,IVa	O	−109 (−129)	IVb,IVa	O	−121 (−12)	[h]	[h]
s2	IVb,IVa	O	−168	IVb,IVa	O	−139 (+47)	[h]	[h]
s1	IVa,IVb	O	−66 (−96)	IVb,IVa	O	−121 (−55)	[h]	[h]
s2	IVa,IVb	O	−140	IVb,IVa	O	−139 (+19)	[h]	[h]

[a]All energies are in kJ mol^{-1} (see Figures S12−S16 for the structures). [b]Oxo species precursor of the corresponding μ-methylene. [c]Symmetry of the surface Re species: T = pseudotetrahedral, P = penta-coordinated, and O = pseudooctahedral. [d]The numbers in parentheses are the adsorption energies of **0-A,B** on **s0**. [e]The energy in parentheses (ΔE) corresponds to the difference in stability of the Re oxo and the μ-methylene species: $\Delta E = E_{ads}(\mu\text{-}CH_2) - E_{ads}$(Re oxo). $E^{\ddagger}$ corresponds to the activation energy from the Re oxo to the corresponding transition-state structure. [f]The numbers in parentheses are the adsorption energies of **1-A,B** on **s0**. [g]The energy in parentheses (ΔE) corresponds to the difference in stability of the alkylidene and the μ-methylene species: $\Delta E = E_{ads}$(alk) − $E_{ads}(\mu\text{-}CH_2)$. [h]No transition state could be located.

ligands; one pointing away from the surface (d(Re−O) = 1.75 Å) and one bound to an Al of the surface with a longer Re−O bond (1.80−1.85 Å, Tables S3−5). The basal plane contains one oxygen ligand bound to the surface and the two carbons of the metallacyclobutane. The TBP metallacycle has a Re−C−C−C dihedral angle close to 0° and a characteristic short Re−β-carbon bond distance (2.38 Å).[14,18,87] In contrast, the SP metallacyclobutanes are puckered with (Re−C−C−C) = 25° and display a long Re−β-carbon bond.[17,19,88] On all sites, the formation of metallacyclobutanes **3** is exoenergetic relative to the alkylidene **2**. When both the SP and TBP isomers were located, the SP isomer is more stable (Table 2 and Figure 4) and formally corresponds to a resting state in the metathesis catalytic cycles.[87] In contrast, the barrier to form **3-SP-A,B** from **2-A,B** and ethylene ($E^{\ddagger}_{2+2\text{-SP}}$) is always much higher than for the formation of **3-TBP-A,B** ($E^{\ddagger}_{2+2\text{-TBP}}$). However, **3-TBP-A,B** can interconvert into **3-SP-A,B** through a turnstile mechanism. Cycloreversion from **3-TBP** or **3-SP** will form **2** and ethylene, which closes the metathesis cycle. Cycloreversion has the same $[TS]^{\ddagger}$ as cycloaddition from microreversibility considerations. The barrier to cycloreversion for **3-SP** is high, and sites that favor formation of **3-SP** through turnstile isomerization will have low activity.

For example, the reaction of **2-III,IVb** and ethylene to form **3-TBP-III,IVb** is favorable (−29 kJ mol^{-1}), and the associated transition state energy is very low ($[TS]^{\ddagger}_{[2+2]\text{-TBP}}$ = +23 kJ mol^{-1}). The transition state energy to form **3-SP-III,IVb** from **2-III,IVb** and ethylene is $[TS]^{\ddagger}_{[2+2]\text{-SP}} = E^{\ddagger}_{[2+2]\text{-SP}}$ = +126 kJ mol^{-1}, and thus is significantly higher than for the formation of **3-TBP-III,IVb** (Table 2 and Figures 4 and S11). **3-TBP-III,IVb** interconverts into **3-SP-III,IVb** with $E^{\ddagger}_{\text{TBP}\rightarrow\text{SP}}$ = +112 kJ mol^{-1}. However, cycloreversion of **3-TBP-III,IVb** has an energy barrier of $E^{\ddagger}_{\text{cyclo}}$ = +52 kJ mol^{-1}. Because the barrier for cycloreversion is lower than for TBP-SP interconversion, **2-III,IVb** sites will be particularly active in metathesis.

2-IVa,IVa and ethylene form **3-TBP-IVa,IVa** with $[TS]^{\ddagger}_{[2+2]\text{-TBP}} = E^{\ddagger}$ = +40 kJ mol^{-1} (Figure S9). The barrier for TBP-SP interconversion is slightly higher ($E^{\ddagger}_{\text{TBP}\rightarrow\text{SP}}$ = +85 kJ mol^{-1}) than for cycloreversion ($E^{\ddagger}_{\text{cyclo}}$ = +77 kJ mol^{-1}). As a result, the formation of the more stable SP metallacycle competes with metathesis on **2-IVa,IVA** sites; hence, this site is less reactive than **2-III,IVb** (Table 2).

Reaction of **2-IVb,IVa** with ethylene yields the seven-coordinate metallacycle **3-IVb,IVa** (ΔE_{ads} = −59 kJ mol^{-1}), but the associated transition state energy is very high $(TS]^{\ddagger}_{[2+2]}$ = +177 kJ mol^{-1}), suggesting that this site will be unreactive in metathesis (Table 2 and Figure S10).

Effect of Partial Hydration of the Surface on CH_3ReO_3/Al_2O_3. Complete dehydration of γ-alumina is not possible without phase transition to θ/α phases.[30] We investigated the effect of one (**s1**) or two (**s2**) water molecules per unit cell (corresponding to 3 and 6 OH nm^{-2}) on the stability, structure, and reactivity of **1**. To have a common reference with the **s0** surface discussed above, Re is attached to the same Al sites, and the proton resulting from the C−H bond activation of the methyl group resides on the same oxygen atom.

*Structure and Relative Energies of **0**, **1**, and **2** Species on **s1** and **s2** Surfaces.* The stability of the mono- and bis-grafted Re oxo species on **III**, **III,IVb**, and **IVa,IVb** was evaluated on **s1** (Table 3). The adsorption energy for **0-III** is −116 kJ mol^{-1}, slightly lower than that on **s0**. **0-III,IVb** and **0-IVa,IVb** have adsorption energies of −184 and −91 kJ mol^{-1}, respectively. The conversion of **0-IVa,IVb** to **1-III,IVb** species has an activation energy of 116 kJ mol^{-1}, whereas the conversion of **0-III** to **1-IVb,III** has a very low activation energy of only 21 kJ mol^{-1}. The formation of **1-IVb,III** from **0-III** is therefore easier than the formation of **1-III,IVb** from **0-IVa,IVb** on both **s0** and **s1** surfaces (Figure S8 for structures).

The adsorption energy of CH_3ReO_3 on alumina to form **1-III,IVb** changes from −233 kJ mol^{-1} on **s0** to −203 kJ mol^{-1} on **s1** and −104 kJ mol^{-1} on **s2**, respectively (Table 3; for the structures, see Figures S12−16). Hence, the μ-methylene species is destabilized with increasing hydroxylation of the surface. The Re−C bonds are elongated by surface hydration from 2.00 Å on **s0** to 2.02 Å on **s1** and 2.11 Å on **s2** (Table S1). A similar trend is observed for the oxo ligand coordinated to the

DOI: 10.1021/jacs.6b00447
J. Am. Chem. Soc. 2016, 138, 6774−6785

surface (1.79 Å on **s0**, 1.78 A on **s1**, and 1.84 Å on **s2**) but not for the Re-oxo pointing away from the surface (1.72 Å for all the three degrees of hydration). The observed variations in bond distances are associated with an increased coordination number at Re, going from 4 (pseudotetrahedral) on both **s0** and **s1** to 5 (distorted trigonal bipyramidal) on **s2**. **1-IVb,III** experiences a similar trend in adsorption energies, going from −211 kJ mol^{-1} on **s0** to −140 and −97 kJ mol^{-1} on **s1** and **s2**, respectively. The coordination numbers at Re follows a similar trend as found for **1-III,IVb**.

The adsorption energy for **1-IVa,IVa** is −90 kJ mol^{-1} on **s0** and only −14 kJ mol^{-1} on **s1**, leading to similar pseudotetrahedral structures. No reasonable low energy structure was found for that site on **s2** because of profound changes of the alumina surface at this level of hydration.[30,31]

The adsorption energy of **1-IVb,IVa** decreases from −129 kJ mol^{-1} on **s0** to −109 kJ mol^{-1} on **s1**. However, it strongly increases on **s2** (E_{ads} = −168 kJ mol^{-1}). **1-IVa,IVb** follows a similar trend with stronger adsorption on **s2** (−140 kJ mol^{-1}) than on **s1** (−66 kJ mol^{-1}) and **s0** (−96 kJ mol^{-1}). In both cases, the pseudo-octahedral geometry of Re is not affected by hydration. Therefore, the stronger adsorption for these hexacoordinated Re μ-methylene probably results from the higher basicity of the surface oxygen atoms coordinated to Re upon adsorption of H_2O on adjacent Al sites.[30,31]

Hydration also decreases the stability of **2-III,IVb** with E_{ads} = −269 kJ mol^{-1} on **s0**, to −193 on **s1**, and −136 kJ mol^{-1} on **s2** (Table 3). **1-III,IVb** is more stable than **2-III,IVb** on **s1** by 10 kJ mol^{-1}. However, **2-III,IVb** is more stable than **1-III,IVb** on **s0** by 36 kJ mol^{-1} and on **s2** by 32 kJ mol^{-1}, indicating that the level of hydration has a nonlinear effect on the relative stability of the methylidene (**2**) and the μ-methylene (**1**) species. On the other sites, hydration leads to similar trends for the relative stability of **1** and **2**. Note that upon hydration the surface becomes more flexible, leading to an increase of the coordination number of the Re center.[31] Indeed, on **s0** and **s1** surfaces, **2-III,IVb** is four-coordinate, whereas on the **s2** surface, it is five-coordinate.

The interconversion of **1-III,IVb** to **2-III,IVb** is associated with high-energy barriers (>150 kJ mol^{-1}) on all surfaces and is unlikely to generate the alkylidene active species as seen in Table 3 (for the structures of the transition states, see Figure S17). In contrast, the interconversion of **1-IVb,III** to **2-III,IVb** becomes nearly barrierless upon hydration (14 kJ mol^{-1} for **s1** and 20 kJ mol^{-1} for **s2** vs 49 kJ mol^{-1} for **s0**). **2-IVa,IVa** has also a lower interconversion energy barrier (66 kJ mol^{-1} for **s1** vs 95 kJ mol^{-1} for **s0**). The TS, starting from either **1-IVb,IVa** or **1-IVa,IVb** to form **1-IVb,IVa**, could not be located.

Although the calculations show that the methylidene (**2**) should be more stable than μ-methylene (**1**) species, except for **III,IVb** on **s1**, only the μ-methylene species are observed experimentally. This discrepancy could arise from the idealized structures of our models compared to the real surface structures. In addition, the alkylidenes have also rather large chemical shift anisotropies (vide infra) and undergo dynamic exchange on the surface, which could prevent detection of these sites using solid-state NMR.[29] However, the computational data show that coadsorption of water and CH_3ReO_3 decreases the stability of tetrahedral Re sites both in their μ-methylene and methylidene forms. In addition, the stability of both sites is leveled out, suggesting that adsorbed water plays a critical role in determining the relative amount of the various species on the various Al sites.[88]

*Reactivity of **1** and **2** and Formation and Structure of Metallacycle **3** on **s1** Surfaces.* The **s1** surface has an OH density (3 OH nm^{-2}) close to the that of experimental surface for dehydroxylation temperatures above 500 °C (<2.5 OH nm^{-2}). The structures of the metallacycles on **s1** are very similar to those on **s0** (Figure S18 and Tables S6 and S7). Cycloaddition, TBP to SP isomerization, and cycloreversion follow trends similar to those on the **s0** surface (Figures S19 and S20 for full metathesis reactions and Figure S21 for the structures of the transition states). On **s1**, the reaction of **2-III,IVb** with ethylene to form **3-TBP-III,IVb** is exoenergetic by 34 kJ mol^{-1} and associated with an energy barrier of +12 kJ mol^{-1}. The TBP to SP interconversion process has a higher barrier than cycloreversion, independent of hydration level. As on the **s0** surface, this site is highly active for metathesis. Also similar to what was calculated for the **s0** surface, **2-IVa,IVa** easily forms the SP metallacycle by a turnstile process from the TBP isomer, indicating that this site is less active than **2-III,IVb**.

The addition of one molecule of water on the surface (**s2**) increases the coordination number of Re to 5 on Al_{III}/Al_{IVb} and Al_{IVa}/Al_{IVa} for methylidene species **2**. In fact, it was not possible to localize a stable **3-TBP-A,B** species (the metathesis active species) on **s2** surface, showing that too high water coverage is detrimental to metathesis activity, as observed experimentally.

NMR Signatures of Surface Sites and Reaction Intermediates. The chemical shift anisotropy (CSA) tensor provides information about the electronic environment at a nucleus, in our case carbon.[29,89] The CSA, in the Herzfeld−Berger convention, is described by the isotropic chemical shift (δ_{iso}, eq 4), the span (Ω, eq 5), and the skew (κ, eq 6), which can be derived from the principal tensor components δ_{11}, δ_{22}, and δ_{33}:[90]

$$\delta_{iso} = (\delta_{11} + \delta_{22} + \delta_{33})/3 \quad (4)$$

$$\Omega = (\delta_{11} - \delta_{33}) \quad (5)$$

$$\kappa = 3(\delta_{22} - \delta_{iso})/\Omega;\ -1 \le \kappa \le +1 \quad (6)$$

δ_{iso} corresponds to the average of δ_{11}, δ_{22}, and δ_{33}, and Ω and κ describe the magnitude of the CSA and the axial symmetry of the tensor, respectively.

The ^{13}C CSA tensors for **1-A,B** and **2-A,B** were calculated, and the results are summarized in Tables 4 and 5. For **1-A,B**, the calculated δ_{iso} of the μ-methylene carbon ranges from 54 to 100 ppm (Table 4), significantly downfield from CH_3ReO_3 (calculated chemical shift of 11 ppm).[91] Octahedral **1-IVa,IVb** and **1-IVb,IVa** have δ_{iso} of 54 and 57 ppm with Ω of ca. 100 ppm. Tetrahedral Re μ-methylene species have δ_{iso} of 82 and 100 ppm with large span values of 128−190 ppm. Sites containing Al_{III} have larger spans than those containing only Al_{IV}. The NMR parameters of **2-A,B** do not depend on the Al

Table 4. Calculated ^{13}C NMR Chemical Shift Anisotropy Tensors (CSA) in ppm (δ_{iso}, Ω and κ) of 1-A,B and 2-A,B on the s0 Al_2O_3 Surface

	1-A,B			2-A,B		
A,B	δ_{iso}	Ω	κ	δ_{iso}	Ω	κ
III,IVb	82	141	0.7	210	405	0.7
IVb,III	100	190	0.8	210	405	0.7
IVa,IVa	88	128	0.8	201	400	0.7
IVb,IVa	57	108	0.4	204	423	0.8
IVa,IVb	54	99	0.7	204	423	0.8

DOI: 10.1021/jacs.6b00447
J. Am. Chem. Soc. 2016, 138, 6774−6785

Table 5. Calculated ^{13}C NMR Chemical Shift Anisotropy Tensors (CSA) in ppm (δ_{iso}, Ω and κ) of 1-A,B and 2-A,B on s1 and s2 Al_2O_3 Surfaces

A,B sites	1-A,B			2-A,B		
	δ_{iso}	Ω	κ	δ_{iso}	Ω	κ
III,IVb−s1	77	121	0.7	228	446	0.7
III,IVb−s2	69	72	0.7	211	414	0.8
IVb,III−s1	82	214	0.8	228	446	0.7
IVb,III−s2	111	192	0.9	211	414	0.8
IVa,IVa−s1	87	170	0.8	216	427	0.7
IVb,IVa−s1	69	119	0.7	232	456	0.7
IVb,IVa−s2	68	122	0.7	222	431	0.7
IVa,IVb−s1	69	136	0.7	232	456	0.7
IVa,IVb−s2	93	140	0.7	222	431	0.7

site: the isotropic chemical shifts are between 201 and 232 ppm with large Ω of 400−456 ppm for all hydration levels (Tables 4 and 5), which is typical for metal alkylidenes.[17] Although methylidene and μ-methylene have very different NMR signatures, the relatively large span and the distribution of sites expected for the alkylidene suggests that they will be more difficult to observe in CH_3ReO_3/Al_2O_3 under standard solid-state NMR conditions (CP-MAS of 10 kHz), especially considering the low amount present on the surface.[29]

The calculated NMR properties of **1** and **2** on **s1** and **s2** are qualitatively similar to those calculated on the **s0** surface (Table 5). For **1-III,IVb**, the structural changes caused by hydration of the surface are accompanied by a decrease of the calculated chemical shift from 82 ppm for **s0** to 77 ppm for **s1** to 69 ppm for **s2**. The span also decreases as hydration increases. In contrast, the chemical shift of **1-IVb,III** is relatively constant upon hydration. However, the span is particularly high on this site and becomes closer to the span of a methylidene ligand (Tables 4 and 5). Experimentally a broad peak centered at 66 ppm was assigned to the **1-A,B** species. We find a reasonable agreement between experiment and calculated chemical shift, the latter ranging from 54 to 111 ppm with most of the values at 50−80 ppm.

The NMR signatures of **3** on the **s0** surface were calculated and are summarized in Table 6. The NMR parameters do not

Table 6. Calculated ^{13}C NMR Chemical Shift Anisotropy Tensors (CSA) in ppm (δ_{iso}, Ω, and κ) of 3 on the s0 Surface

A,B		3-TBP-A,B			3-SP-A,B		
		δ_{iso}	Ω	κ	δ_{iso}	Ω	κ
III,IVb	α	105	168	0.2	56	65	0.2
	β	16	84	0.6	35	15	0.3
IVa,IVa	α	105	175	0.3	42	43	0.4
	β	16	90	0.6	29	25	0.8
IVb,IVa	α	*a*	*a*	*a*	67	87	0.2
	β	*a*	*a*	*a*	39	14	0.6

[a]TBP metallacyclobutane could not be located on Al_{IVb},Al_{IVa}.

vary much between Al sites but are characteristic of the geometry of the metallacycle. The isotropic chemical shift of the α-carbon in **3-TBP** is 105 ppm, with spans ranging from 168 to 175 ppm. The calculated isotropic shift for the β-carbon in **3-TBP** is 16 ppm with a span of 84−90 ppm. Experimentally, we found chemical shifts of 120 ppm for the α-carbon of **3-TBP** and 19 ppm for the β-carbon of **3-TBP** which is in very good agreement with calculations. For **3-SP**, the isotropic chemical shifts of the α- and β-carbons range from 29−67 ppm, again in good agreement with the 43/36 ppm found in the experiment.

The span of the β-carbons in **3-SP** are larger than those of the α-carbons. These data indicate that the NMR properties of the TBP and SP isomers are different and distinguishable by NMR spectroscopy as found experimentally for isoelectronic Mo and W complexes.[17,19,88] Surface hydration has almost no effect on the chemical shift anisotropy tensor of metallacyclobutane **3-SP** and **3-TBP** (Table S8).

Relationship between NMR Signature and Reactivity. The most active metathesis site (**1-IVb,III**) displays a very specific NMR signature, in particular a larger calculated span than any other site. We therefore analyzed the projected density of state (PDOS) of the s and p orbitals of the C atom in **1-III,IVb**, **1-IVb,III**, and **2-III,IVb** (Table 7) and compared it with that of

Table 7. Position of the HOMO in the PDOS Graph for the Methylidene (2-A,B) and the μ-Methylene (1-A,B) Species Formed on Al_{III} and Al_{IVb} Sites on the s0, s1, and s2 Surfaces

species	p orbital position in PDOS graph (in eV)[a]
	s0 Surface
2-III,IVb	−5.64
1-IVb,III	−6.72
1-III,IVb	−6.87 (minor) and −7.19
	s1 Surface
2-III,IVb	−5.61
1-IVb,III	−6.26 and −6.58
1-III,IVb	−6.58 (minor) and −7.23
	s2 Surface
2-III,IVb	−5.02
1-IVb,III	−5.73
1-III,IVb	−6.70 and −7.02

[a]To allow a comparison between the surfaces, the vacuum potential (plane-average electrostatic potential of an electron in the *z* direction) of the unit cell far from the surface for every adsorbate−surface system was used as reference value.

CH_3ReO_3 and its enolic form $CH_2Re(OH)O_2$. The HOMO is essentially composed of the p orbitals perpendicular to the CH_2 plane for the molecular Re complex (Figures S22−24). In CH_3ReO_3/Al_2O_3, a similar pattern of peaks arises, but these peaks are shifted. By comparing the HOMO energy of the grafted fragments in **1-IVb,III** and **1-III,IVb** with those of corresponding methylidenes (**2-III,IVb**), we can define the methylidene character of the μ-methylene species; the closer the energies of μ-methylene and methylidene, the higher the methylidene character. The energy of the HOMO (with main p character on C) in the PDOS for **1-IVb,III**, **1-III,IVb**, and **2-III,IVb** is reported as a function of surface hydration in Table 7. The compilation of the PDOS for all the previously described μ-methylene and methylidene species on all the Al sites can be found in Figures S25−S40.

On the **s0** surface, the energy of the HOMO p orbital in **2-III,IVb** is −5.64 eV (Table 7). The HOMO of p character in **1-IVb,III** is closer in energy to **2-III,IVb** than the corresponding orbital in **1-III,IVb**. This suggests that **1-IVb,III** species have a higher alkylidene character than that of **1-III,IVb** species. As the surface becomes hydrated, the HOMO in **2-III,IVb** shifts to higher energies. A similar shift to higher energies is also experienced by the HOMOs of **1-IVb,III** and **1-III,IVb**. The HOMO in **1-IVb,III** on the **s2** surface is at −5.73 eV, significantly closer in energy to that of **2-III,IVb** (−5.02 eV)

DOI: 10.1021/jacs.6b00447
J. Am. Chem. Soc. 2016, 138, 6774−6785

than **1-III,IVb** (−6.70 eV). Overall, **1-IVb,III** has more alkylidene character than **1-III,IVb**, in particular on the **s1** and **s2** surfaces.

DISCUSSION

Activation of alumina above 500 °C (≤4 OH·nm^{-2}) is an essential step to obtain active CH_3ReO_3/Al_2O_3 metathesis catalysts. Titration of active sites with ^{13}C-dilabeled ethylene and NMR spectroscopy of CH_3ReO_3/Al_2O_3 indicated a distribution of Re sites in these catalysts. Although no alkylidene species could be observed, metallacycle intermediates were detected by solid-state NMR spectroscopy in the presence of ^{13}C-labeled ethylene.

DFT calculations showed that bis-Re oxo (**0-A,B**) and μ-methylene (**1-A,B**) species are accessible. **1-A,B** forms by the activation of a C−H bond in $MeReO_3$ across a surface Al,O bond. In **1-A,B**, aluminum A coordinates to μ-methylene and B to Re═O; a proton is present on a nearby O atom. **1-III,IVb** is the thermodynamically preferred μ-methylene species for all the hydroxylation levels studied (**s0**, **s1**, and **s2** surfaces). Although **1-IVb,III** is slightly less stable (by 22 and 63 kJ mol^{-1} for **s0** and **s1**, respectively), it is the kinetically preferred μ-methylene (obtained through pathways with lower activation energies). Considering the experimental conditions and the nonuniform hydroxylation state of alumina,[92] a mixture of dioxo-grafted and μ-methylene species on the various Al sites is expected to be formed.

A first question to answer is the origin of the low activity of CH_3ReO_3 on alumina pretreated at a temperature of only 300 °C. At this temperature the Al_{III} defect sites of Al_2O_3 are occupied by water molecules and are not accessible to bind N_2 or activate H_2 or CH_4.[30,31] The reason for the activity of CH_3ReO_3 supported on alumina activated at 300 °C can be understood by the coadsorption energy (E_{coads}) of CH_3ReO_3 and ***i*** water molecules per unit cell, taking the **s0** surface as reference (eq 7). It allows comparing the stability of isomers and to check whether adsorption of water is less or more favorable than that of CH_3ReO_3:

$$E_{coads} = E(\mathbf{s}i + CH_3ReO_3) - E(CH_3ReO_3) - i \times E(H_2O) - E(\mathbf{s0}) \quad (7)$$

where **s*i*** defines the surface with water molecules and ***i*** defines the number of H_2O molecules. When no CH_3ReO_3 is present, this equation simplifies to

$$E_{coads} = E(\mathbf{s}i) - i^{*}E(H_2O) - E(\mathbf{s0}) \quad (8)$$

The calculated energies of coadsorption of CH_3ReO_3 and water on the alumina sites (E_{coads}) are reported in Table 8.[31] E_{coads} of CH_3ReO_3 and H_2O is stronger than the adsorption of water alone. From a thermodynamic point of view, if the most Lewis acidic sites are occupied by adsorbed water, then CH_3ReO_3 should be able to displace H_2O to generate the μ-methylene sites (Table 8). This is supported by experimental observations. For example, μ-methylene species **II** is observed by NMR spectroscopy on alumina dehydroxylated at 300 °C (Figure S41). In addition, a broad OH-band is observed by IR spectroscopy upon adsorption of CH_3ReO_3, suggesting restructuration of surface OH upon adsorption of CH_3ReO_3 on Al_2O_3.[28,56]

Table 8. Coadsorption Energy (kJ mol^{-1}) of 1-III,IVb, 1-IVb,III, and Water as a Function of OH Coverage on Alumina Surface

water coverage (OH nm^{-2})	E_{coads} **1-III,IVb**	E_{coads} **1-IVb,III**	E_{coads} H_2O
0	−233	−211	0
3	−373	−318	−226
6	−503	−496	−406

A second question concerns the presence of different μ-methylene sites and their different activity in metathesis. The isomerization of the μ-methylene **1-III,IVb** into the methylidene **2-III,IVb** is associated with a very high energy barrier (200 kJ mol^{-1} for **s0**, 199 kJ mol^{-1} for **s1**, and 156 kJ mol^{-1} for **s2**), indicating that metathesis is unlikely at this site. **1-IVb,IVa** and **1-IVa,IVb** are calculated to be unreactive because of very high energy barriers for [2 + 2] cycloaddition. These results are consistent with the experimental observation that some μ-methylene species do not react with ethylene. Of the other possible combinations, **1-IVa,IVa** can kinetically form active species. Although the adsorption of CH_3ReO_3 on two adjacent Al_{IVa} sites is not associated with particularly high adsorption energies (−90 kJ mol^{-1} on **s0** and −51 kJ mol^{-1} on **s1**), Al_{IVa} sites are typically free of adsorbed H_2O at low OH coverage.[31] However, on these sites, TBP metallacycle easily interconvert into the more stable and less reactive SP isomer, which will lead to less active sites.

The third question is the optimal structure for the active sites for metathesis. **1-IVb,III** is only slightly less thermodynamically stable than **1-III,IVb**. However, interconversion of **1-IVb,III** into **2-III,IVb** has a low barrier. Subsequent [2 + 2] cycloaddition of **2-III,IVb** and ethylene to form TBP metallacyclobutane and cycloreversion have low barriers on this site. Equally important is the TBP to SP interconversion—a source of resting-state SP metallacycles—has a higher barrier than cycloreversion making that site particularly active for metathesis.

The computational data suggests that the TBP and SP metallacycles observed by NMR spectroscopy are associated with **1-IVb,III** and **1-IVa,IVa** sites, respectively. The computational data also indicates that the "defect" sites in alumina (Al_{III}) are key to generate highly active sites. From the computed catalytic reactions, the metathesis activity of the different μ-methylene sites will follow this order: **1-IVb,III** > **1-IVa,IVa** ≫ **1-III,IVb**, **1-IVb,IVa**, **1-IVa,IVb**.

A characteristic feature of each μ-methylene site is the calculated span value of the μ-CH_2. The largest span values were computed for the most active site **1-IVb,III**. Comparison of the PDOS of active **1-IVb,III**, inactive **1-III,IVb**, and alkylidene **2-III,IVb** showed that **1-IVb,III** has methylidene character and is therefore more apt to generate the active sites. Taken together, the data presented here show that the combination of Al_{III} and Al_{IVb} sites are essential for metathesis activity and that adsorbed water assists the formation of active sites.

Finally, the fourth question concerns the optimal treatment of the alumina support. The presence of one adsorbed water molecule per unit cell (**s1**, 3 OH·nm^{-2}) leads to both easier formation of **1-IVb,III** and easier [2 + 2] cycloreversion, compared to that of the fully dehydroxylated **s0** surface. Additional water molecules (**s2** surface) destabilize **1-A,B** and generate penta-coordinated Re surface species, consistent with the decrease in catalyst performance with alumina dehydroxylated at lower temperature (<500 °C, >6 OH·nm^{-2}) and the finding of an optimal activity at intermediate coverage.

DOI: 10.1021/jacs.6b00447
J. Am. Chem. Soc. 2016, 138, 6774−6785

CONCLUSIONS

The resting state leading to the most active catalytic intermediate in the CH_3ReO_3/Al_2O_3 alkene metathesis catalyst is **1-IVb,III**. This μ-methylene species contains a tetracoordinate Re oxo center bound to the alumina surface through two bonds: one between Al_{IVb} and C and another between an Al_{III} site and an oxo ligand. The analysis of the projected density of state (PDOS) shows that the μ-methylene species on **1-IVb,III** has a stronger methylidene character than that of other sites. **1-IVb,III** is optimal because it can readily interconvert into the corresponding methylidene isomer, which is the catalytically active species forming with ethene the metallacyclobutane through a very low barrier (23 kJ mol^{-1}). In addition, this site allows fast cycloreversion, rather than interconversion into the more stable SP isomer. Other less active μ-methylene species can also be formed, hence explaining the distribution of site strength on the catalyst and the presence of unreacted μ-methylene after reaction. This study also explains the role of preactivation temperature on metathesis activity. As the temperature increases, the density of OH groups decreases, freeing Al_{III} sites to interact with CH_3ReO_3 instead of water. The presence of some adsorbed water (<3 OH nm^{-2}) increases the flexibility of the surface, resulting in a decrease of the activation barrier for the formation of methylidene and TBP metallacyclobutane intermediates. The presence of too much adsorbed water (>6 OH nm^{-2}) destabilizes the formation of μ-methylene species. The existence of an optimal pretreatment temperature for the alumina support used in the preparation of the CH_3ReO_3/Al_2O_3 catalyst and the need for Lewis acidic Al_{III} sites parallels what was found for Re_2O_7/Al_2O_3. Overall, this is strong evidence for the essential role of Al_{III} "defect" sites in industrial Re-based metathesis catalysts.

ASSOCIATED CONTENT

Supporting Information

The Supporting Information is available free of charge on the ACS Publications website at DOI: 10.1021/jacs.6b00447.

Catalytic activity data; $^1H-^{13}C$ CPMAS NMR and $^1H-^{13}C$ HETCOR NMR spectra; bond lengths and angles; structure, transition state, and stability data, method of calculation of bond angles; calculated structures; NMR shift parameters; PDOS spectra; and occupied molecular orbitals. (PDF)

AUTHOR INFORMATION

Corresponding Authors

*E-mail: ccoperet@ethz.ch.
*E-mail: philippe.sautet@ens-lyon.fr.

Present Address

R.W.: Eco-Efficient Products and Processes Laboratory (E2P2L), UMI 3464 CNRS−Solvay, 3966 Jin Du Road, Xin Zhuang Ind. Zone, 201108 Shanghai, China.

Notes

The authors declare no competing financial interest.

ACKNOWLEDGMENTS

M.V. and A.C.-V. thank the SNF foundation for financial support (Grant No. 200021_142600 and Ambizione Project PZ00P2_148059, respectively).

REFERENCES

(1) Banks, R. L.; Bailey, G. C. *Ind. Eng. Chem. Prod. Res. Dev.* **1964**, *3*, 170.
(2) Chauvin, Y.; Commereuc, D. *J. Chem. Soc., Chem. Commun.* **1992**, 462.
(3) Ivin, K. J.; Mol, J. C. *Olefin Metathesis and Metathesis Polymerization*; Academic Press: San Diego, CA, 1997
(4) Lwin, S.; Wachs, I. E. *ACS Catal.* **2014**, *4*, 2505.
(5) Schrock, R. R. *Angew. Chem., Int. Ed.* **2006**, *45*, 3748.
(6) Murdzek, J. S.; Schrock, R. R. *Organometallics* **1987**, *6*, 1373.
(7) Schrock, R. R.; Murdzek, J. S.; Bazan, G. C.; Robbins, J.; DiMare, M.; O'Regan, M. *J. Am. Chem. Soc.* **1990**, *112*, 3875.
(8) Nguyen, S. T.; Johnson, L. K.; Grubbs, R. H.; Ziller, J. W. *J. Am. Chem. Soc.* **1992**, *114*, 3974.
(9) Scholl, M.; Ding, S.; Lee, C. W.; Grubbs, R. H. *Org. Lett.* **1999**, *1*, 953.
(10) Hoveyda, A. H. *J. Org. Chem.* **2014**, *79*, 4763.
(11) Lawrenson, M. J. U.S. Patent US3974233A, 1976.
(12) Mol, J. C. *Catal. Today* **1999**, *51*, 289.
(13) Mol, J. C. *J. Mol. Catal. A: Chem.* **2004**, *213*, 39.
(14) Feldman, J.; Davis, W. M.; Schrock, R. R. *Organometallics* **1989**, *8*, 2266.
(15) Feldman, J.; Davis, W. M.; Thomas, J. K.; Schrock, R. R. *Organometallics* **1990**, *9*, 2535.
(16) Solans-Monfort, X.; Clot, E.; Copéret, C.; Eisenstein, O. *J. Am. Chem. Soc.* **2005**, *127*, 14015.
(17) Blanc, F.; Berthoud, R.; Copéret, C.; Lesage, A.; Emsley, L.; Singh, R.; Kreickmann, T.; Schrock, R. R. *Proc. Natl. Acad. Sci. U. S. A.* **2008**, *105*, 12123.
(18) Solans-Monfort, X.; Copéret, C.; Eisenstein, O. *Organometallics* **2012**, *31*, 6812.
(19) Mougel, V.; Copéret, C. *Chem. Sci.* **2014**, *5*, 2475.
(20) Mougel, V.; Santiago, C. B.; Zhizhko, P. A.; Bess, E. N.; Varga, J.; Frater, G.; Sigman, M. S.; Copéret, C. *J. Am. Chem. Soc.* **2015**, *137*, 6699.
(21) Popoff, N.; Mazoyer, E.; Pelletier, J.; Gauvin, R. M.; Taoufik, M. *Chem. Soc. Rev.* **2013**, *42*, 9035.
(22) Tian, H.; Roberts, C. A.; Wachs, I. E. *J. Phys. Chem. C* **2010**, *114*, 14110.
(23) Debecker, D. P.; Stoyanova, M.; Rodemerck, U.; Gaigneaux, E. M. *J. Mol. Catal. A: Chem.* **2011**, *340*, 65.
(24) Imamoğlu, Y., Ed. *Metathesis Polymerization of Olefins and Polymerization of Alkynes*; Kluwer Academic: Boston, MA, 1998.
(25) Moffat, A. J.; Clark, A.; Johnson, M. M. *J. Catal.* **1971**, *22*, 379.
(26) Copéret, C.; Chabanas, M.; Petroff Saint-Arroman, R.; Basset, J.-M. *Angew. Chem., Int. Ed.* **2003**, *42*, 156.
(27) Rhers, B.; Salameh, A.; Baudouin, A.; Quadrelli, E. A.; Taoufik, M.; Copéret, C.; Lefebvre, F.; Basset, J.-M.; Solans-Monfort, X.; Eisenstein, O.; Lukens, W. W.; Lopez, L. P. H.; Sinha, A.; Schrock, R. R. *Organometallics* **2006**, *25*, 3554.
(28) Salameh, A.; Joubert, J.; Baudouin, A.; Lukens, W.; Delbecq, F.; Sautet, P.; Basset, J. M.; Copéret, C. *Angew. Chem., Int. Ed.* **2007**, *46*, 3870.
(29) Blanc, F.; Basset, J.-M.; Copéret, C.; Sinha, A.; Tonzetich, Z. J.; Schrock, R. R.; Solans-Monfort, X.; Clot, E.; Eisenstein, O.; Lesage, A.; Emsley, L. *J. Am. Chem. Soc.* **2008**, *130*, 5886.
(30) Wischert, R.; Copéret, C.; Delbecq, F.; Sautet, P. *Angew. Chem., Int. Ed.* **2011**, *50*, 3202.
(31) Wischert, R.; Laurent, P.; Copéret, C.; Delbecq, F.; Sautet, P. *J. Am. Chem. Soc.* **2012**, *134*, 14430.
(32) Conley, M. P.; Mougel, V.; Peryshkov, D. V.; Forrest, W. P.; Gajan, D.; Lesage, A.; Emsley, L.; Copéret, C.; Schrock, R. R. *J. Am. Chem. Soc.* **2013**, *135*, 19068.
(33) Yermakov, Y. I. In *Studies in Surface Science and Catalysis*; Seivama, T., Tanabe, K., Eds.; Elsevier: New York, 1981; Vol. 7, Part A, p 57.
(34) Guzman, J.; Gates, B. C. *Dalton Trans.* **2003**, 3303.

DOI: 10.1021/jacs.6b00447
J. Am. Chem. Soc. 2016, 138, 6774−6785

(35) Copéret, C.; Comas-Vives, A.; Conley, M. P.; Estes, D.; Fedorov, A.; Mougel, V.; Nagae, H.; Núñez-Zarur, F.; Zhizhko, P. *Chem. Rev.* **2016**, *116*, 323.
(36) Rascon, F.; Wischert, R.; Coperet, C. *Chem. Sci.* **2011**, *2*, 1449.
(37) Stalzer, M.; Delferro, M.; Marks, T. *Catal. Lett.* **2015**, *145*, 3.
(38) Tada, M.; Iwasawa, Y. *Coord. Chem. Rev.* **2007**, *251*, 2702.
(39) Chabanas, M.; Baudouin, A.; Copéret, C.; Basset, J.-M. *J. Am. Chem. Soc.* **2001**, *123*, 2062.
(40) Chabanas, M.; Copéret, C.; Basset, J.-M. *Chem. - Eur. J.* **2003**, *9*, 971.
(41) Copéret, C. *Dalton Trans.* **2007**, 5498.
(42) Rendón, N.; Berthoud, R.; Blanc, F.; Gajan, D.; Maishal, T.; Basset, J.-M.; Copéret, C.; Lesage, A.; Emsley, L.; Marinescu, S. C.; Singh, R.; Schrock, R. R. *Chem. - Eur. J.* **2009**, *15*, 5083.
(43) Gajan, D.; Rendon, N.; Wampler, K. M.; Basset, J.-M.; Copéret, C.; Lesage, A.; Emsley, L.; Schrock, R. R. *Dalton Trans.* **2010**, *39*, 8547.
(44) Copéret, C. *Beilstein J. Org. Chem.* **2011**, *7*, 13.
(45) Conley, M. P.; Forrest, W. P.; Mougel, V.; Copéret, C.; Schrock, R. R. *Angew. Chem., Int. Ed.* **2014**, *53*, 14221.
(46) Valla, M.; Stadler, D.; Mougel, V.; Copéret, C. *Angew. Chem., Int. Ed.* **2016**, *55*, 1124.
(47) Mougel, V.; Copéret, C. *ACS Catal.* **2015**, *5*, 6436.
(48) Lwin, S.; Keturakis, C.; Handzlik, J.; Sautet, P.; Li, Y.; Frenkel, A. I.; Wachs, I. E. *ACS Catal.* **2015**, *5*, 1432.
(49) Lwin, S.; Wachs, I. E. *ACS Catal.* **2015**, *5*, 6823.
(50) Verkuijlen, E.; Kapteijn, F.; Mol, J. C.; Boelhouwer, C. *J. Chem. Soc., Chem. Commun.* **1977**, 198.
(51) Wohrle, I.; Reckziegel, A.; Esser, P.; Sturmann, M. U.S. Patent US20030054956 A1, 2001.
(52) Salameh, A.; Baudouin, A.; Basset, J. M.; Copéret, C. *Angew. Chem., Int. Ed.* **2008**, *47*, 2117.
(53) Herrmann, W. A.; Wagner, W.; Flessner, U.; Volkhardt, U.; Komber, H. *Angew. Chem.* **1991**, *103*, 1704.
(54) Buffon, R.; Auroux, A.; Lefebvre, F.; Leconte, M.; Choplin, A.; Basset, J. M.; Herrmann, W. A. *J. Mol. Catal.* **1992**, *76*, 287.
(55) Rost, A. M. J.; Schneider, H.; Zoller, J. P.; Herrmann, W. A.; Kuhn, F. E. *J. Organomet. Chem.* **2005**, *690*, 4712.
(56) Salameh, A.; Baudouin, A.; Soulivong, D.; Boehm, V.; Roeper, M.; Basset, J.-M.; Copéret, C. *J. Catal.* **2008**, *253*, 180.
(57) Moses, A. W.; Raab, C.; Nelson, R. C.; Leifeste, H. D.; Ramsahye, N. A.; Chattopadhyay, S.; Eckert, J.; Chmelka, B. F.; Scott, S. L. *J. Am. Chem. Soc.* **2007**, *129*, 8912.
(58) Verkuijlen, E.; Kapteijn, F.; Mol, J. C.; Boelhouwer, C. *J. Chem. Soc., Chem. Commun.* **1977**, 198.
(59) Valla, M.; Conley, M. P.; Copéret, C. *Catal. Sci. Technol.* **2015**, *5*, 1438.
(60) Wischert, R.; Copéret, C.; Delbecq, F.; Sautet, P. *ChemCatChem* **2010**, *2*, 812.
(61) Handzlik, J.; Sautet, P. *J. Phys. Chem. C* **2010**, *114*, 19406.
(62) Herrmann, W. A.; Kuehn, F. E.; Fischer, R. W.; Thiel, W. R.; Romao, C. C. *Inorg. Chem.* **1992**, *31*, 4431.
(63) Perdew, J. P.; Wang, Y. *Phys. Rev. B: Condens. Matter Mater. Phys.* **1992**, *45*, 13244.
(64) Kresse, G.; Furthmüller, J. *Phys. Rev. B: Condens. Matter Mater. Phys.* **1996**, *54*, 11169.
(65) Kresse, G.; Furthmüller, J. *Comput. Mater. Sci.* **1996**, *6*, 15.
(66) Blöchl, P. E. *Phys. Rev. B: Condens. Matter Mater. Phys.* **1994**, *50*, 17953.
(67) Henkelman, G.; Uberuaga, B. P.; Jónsson, H. *J. Chem. Phys.* **2000**, *113*, 9901.
(68) Henkelman, G.; Jónsson, H. *J. Chem. Phys.* **2000**, *113*, 9978.
(69) Clark, S. J.; Segall, M. D.; Pickard, C. J.; Hasnip, P. J.; Probert, M. I. J.; Refson, K.; Payne, M. C. *Z. Kristallogr. - Cryst. Mater.* **2005**, *220*, 567.
(70) Perdew, J. P.; Burke, K.; Ernzerhof, M. *Phys. Rev. Lett.* **1996**, *77*, 3865.
(71) Perdew, J. P.; Burke, K.; Ernzerhof, M. *Phys. Rev. Lett.* **1997**, *78*, 1396.
(72) Kokalj, A. *J. Mol. Graphics Modell.* **1999**, *17*, 176.
(73) Frisch, M. J.; Trucks, G. W.; Schlegel, H. B.; Scuseria, G. E.; Robb, M. A.; Cheeseman, J. R.; Scalmani, G.; Barone, V.; Mennucci, B.; Petersson, G. A.; Nakatsuji, H.; Caricato, M.; Li, X.; Hratchian, H. P.; Izmaylov, A. F.; Bloino, J.; Zheng, G.; Sonnenberg, J. L.; Hada, M.; Ehara, M.; Toyota, K.; Fukuda, R.; Hasegawa, J.; Ishida, M.; Nakajima, T.; Honda, Y.; Kitao, O.; Nakai, H.; Vreven, T.; Montgomery, J. A., Jr.; Peralta, J. E.; Ogliaro, F.; Bearpark, M.; Heyd, J. J.; Brothers, E.; Kudin, K. N.; Staroverov, V. N.; Kobayashi, R.; Normand, J.; Raghavachari, K.; Rendell, A.; Burant, J. C.; Iyengar, S. S.; Tomasi, J.; Cossi, M.; Rega, N.; Millam, J. M.; Klene, M.; Knox, J. E.; Cross, J. B.; Bakken, V.; Adamo, C.; Jaramillo, J.; Gomperts, R.; Stratmann, R. E.; Yazyev, O.; Austin, A. J.; Cammi, R.; Pomelli, C.; Ochterski, J. W.; Martin, R. L.; Morokuma, K.; Zakrzewski, V. G.; Voth, G. A.; Salvador, P.; Dannenberg, J. J.; Dapprich, S.; Daniels, A. D.; Farkas, O.; Foresman, J. B.; Ortiz, J. V.; Cioslowski, J.; Fox, D. J. *Gaussian 09*, revision D.01; Gaussian, Inc.: Wallingford, CT, 2009.
(74) Becke, A. D. *J. Chem. Phys.* **1993**, *98*, 5648.
(75) Hay, P. J.; Wadt, W. R. *J. Chem. Phys.* **1985**, *82*, 299.
(76) Ehlers, A. W.; Böhme, M.; Dapprich, S.; Gobbi, A.; Höllwarth, A.; Jonas, V.; Köhler, K. F.; Stegmann, R.; Veldkamp, A.; Frenking, G. *Chem. Phys. Lett.* **1993**, *208*, 111.
(77) Joubert, J.; Salameh, A.; Krakoviack, V.; Delbecq, F.; Sautet, P.; Copéret, C.; Basset, J. M. *J. Phys. Chem. B* **2006**, *110*, 23944.
(78) Grinev, V. E.; Khalif, V. A.; Aptekar', E. L.; Krylov, O. V. *Bull. Acad. Sci. USSR, Div. Chem. Sci.* **1981**, *30*, 1338.
(79) Grinev, V. E.; Madden, M.; Khalif, V. A.; Aptekar', E. L.; Aldag, A. W.; Krylov, O. V. *Kinet. Catal.* **1983**, *24*, 641.
(80) Flatt, B. T.; Grubbs, R. H.; Blanski, R. L.; Calabrese, J. C.; Feldman, J. *Organometallics* **1994**, *13*, 2728.
(81) Toreki, R.; Vaughan, G. A.; Schrock, R. R.; Davis, W. M. *J. Am. Chem. Soc.* **1993**, *115*, 127.
(82) Webber, A. L.; Elena, B.; Griffin, J. M.; Yates, J. R.; Pham, T. N.; Mauri, F.; Pickard, C. J.; Gil, A. M.; Stein, R.; Lesage, A.; Emsley, L.; Brown, S. P. *Phys. Chem. Chem. Phys.* **2010**, *12*, 6970.
(83) Salager, E.; Stein, R. S.; Steuernagel, S.; Lesage, A.; Elena, B.; Emsley, L. *Chem. Phys. Lett.* **2009**, *469*, 336.
(84) Digne, M.; Sautet, P.; Raybaud, P.; Euzen, P.; Toulhoat, H. *J. Catal.* **2002**, *211*, 1.
(85) Digne, M.; Sautet, P.; Raybaud, P.; Euzen, P.; Toulhoat, H. *J. Catal.* **2004**, *226*, 54.
(86) Krokidis, X.; Raybaud, P.; Gobichon, A. E.; Rebours, B.; Euzen, P.; Toulhoat, H. *J. Phys. Chem. B* **2001**, *105*, 5121.
(87) Solans-Monfort, X.; Copéret, C.; Eisenstein, O. *J. Am. Chem. Soc.* **2010**, *132*, 7750.
(88) Solans-Monfort, X.; Copéret, C.; Eisenstein, O. *Organometallics* **2015**, *34*, 1668.
(89) Duer, M. J., Ed. *Solid-State NMR Spectroscopy: Principles and Applications*; Blackwell Science: Oxford, U.K., 2002; p 216.
(90) Herzfeld, J.; Berger, A. E. *J. Chem. Phys.* **1980**, *73*, 6021.
(91) Herrmann, W. A.; Scherer, W.; Fischer, R. W.; Blumel, J.; Kleine, M.; Mertin, W.; Gruehn, R.; Mink, J.; Boysen, H. *J. Am. Chem. Soc.* **1995**, *117*, 3231.
(92) Metivier, R.; Leray, I.; Roy-Auberger, M.; Zanier-Szydlowski, N.; Valeur, B. *New J. Chem.* **2002**, *26*, 411.

DOI: 10.1021/jacs.6b00447
J. Am. Chem. Soc. 2016, 138, 6774−6785